

Di-photon resonance around 750 GeV: shedding light on the theory underneath[☆]

Joydeep Chakraborty^a, Arghya Choudhury^{b,c}, Pradipta Ghosh^{d,e}, Subhadeep Mondal^f, Tripurari Srivastava^a

^aDepartment of Physics, Indian Institute of Technology, Kanpur-208016, India

^bConsortium for Fundamental Physics, Department of Physics and Astronomy,
University of Sheffield, Sheffield S3 7RH, United Kingdom

^cConsortium for Fundamental Physics, Department of Physics and Astronomy,
University of Manchester, Manchester, M13 9PL, United Kingdom

^dLaboratoire de Physique Théorique, CNRS¹, Univ. Paris-Sud, Université Paris-Saclay, 91405 Orsay, France

^eCentre de Physique Théorique, École polytechnique, CNRS², Université Paris-Saclay, 91128 Palaiseau, France

^fRegional Centre for Accelerator-based Particle Physics, Harish-Chandra Research Institute, Allahabad 211019, India

Abstract

Both the ATLAS and CMS collaborations have recently observed an excess in the di-photon invariant mass distribution in the vicinity of 750 GeV with a local significance of $\sim 3\sigma$. In this article we try to investigate this excess in the context of a minimal simplified framework assuming effective interactions of the hinted resonance with photons and gluons. We scrutinise the consistency of this observation with possible accompanying yet hitherto unseen signatures of this resonance. Subsequently, we try to probe the nature of new particles, e.g., spin, electric charge and number of colour, etc., that could remain instrumental to explain this excess through loop-mediation.

The recent observation by the LHC collaborations [1, 2, 3, 4], concerning an excess in the di-photon invariant mass distribution $m_{\gamma\gamma}^{inv}$ near 750 GeV, has gained huge attention in the particle physics community. The ATLAS group, using 3.2 fb^{-1} of data with 13 TeV centre-of-mass energy (E_{CM}), has estimated a local (global) significance of 3.9σ (2.0σ) for a mass of the resonance $M_X = 750 \text{ GeV}$ [3]. At the same time, the CMS collaboration has noticed a local (global) significance of $2.8\sigma - 2.9\sigma$ ($< 1.0\sigma$) for $M_X = 760 \text{ GeV}$ [4] using 3.3 fb^{-1} of data at $E_{CM} = 13 \text{ TeV}$. Combining with the run-I data (19.7 fb^{-1} at $E_{CM} = 8 \text{ TeV}$), the CMS excess appears at $M_X = 750 \text{ GeV}$ [4] with a local (global) significance of 3.4σ (1.6σ). The latter corresponds to a narrow width for the resonance, $\Gamma_X = 105 \text{ MeV}$ while interpretation with only 13 TeV data indicates $\Gamma_X = 10.6 \text{ GeV}$. The ATLAS measurement, on the contrary, hints a large decay width $\Gamma_X = 45 \text{ GeV}$ [3].

This is the first surprise from LHC run-II with 13 TeV center-of-mass energy³ which remains unexplained within the Standard Model (SM) framework. In other words, properties of the said resonance, as experimentally observed so far, e.g., excess in $\gamma\gamma$ only and nothing in ZZ , $Z\gamma$ or in di-jet (jj) channels, definitely demand physics beyond the SM (BSM). It is,

thus, timely to explore the origin and associated consequences of this resonance although the possibility of loosing this excess with more data-set can not be completely overlooked. A quest to accommodate this excess has already produced a handful of contemporary analyses [7, 8, 9, 10, 11, 12, 13, 14, 15, 16, 17, 18, 19, 20, 21, 22, 23, 24] along with a few simultaneous⁴ [25, 26, 27, 28, 29] studies. Most of these analyses are proposed within the context of a specific theory framework, which often requires new decay modes (invisible for example) and thus, address other issues, for example the dark matter (see Refs. [8, 9]). We, however, aim to investigate this excess with a simplified effective framework and will try to explore the nature of hitherto unseen particles which, while running in the loop, can appear instrumental to produce the observed di-photon excess.

With this idea we have used a generic Lagrangian which couples this new resonance H_X with photons and gluons as shown by eq. (1). We have further assumed: (1) *on-shell* production of H_X and (2) a scalar, i.e., spin-0, nature⁵ for H_X . The latter is one of the natural options to explain a resonance in di-photon channel, i.e., two *identical massless spin-1* particles, as dictated by Landau-Yang theorem [30, 31]. The effective minimal⁶ Lagrangian is written as:

$$\mathcal{L}_{eff} = \kappa_g G_{\mu\nu}^a G_a^{\mu\nu} H_X + \kappa_A B_{\mu\nu} B^{\mu\nu} H_X, \quad (1)$$

where $G_{\mu\nu}^a$, $B_{\mu\nu}$ are the associated field strengths with “a” representing the relevant non-Abelian index. The effective H_X -g-g

[☆]LPT-Orsay-15-101, CPHT-RR060.1215, HRI-RECAPP-2015-020

Email addresses: joydeep@iitk.ac.in (Joydeep Chakraborty),
a.choudhury@sheffield.ac.uk (Arghya Choudhury),
pradipta.ghosh@th.u-psud.fr (Pradipta Ghosh),
subhadeepmondal@hri.res.in (Subhadeep Mondal),
tripurar@iitk.ac.in (Tripurari Srivastava)

¹UMR 8627

²UMR 7644

³A *less significant* increasing fluctuation was also noticed during the LHC run-I with 8 TeV center-of-mass energy [5, 6].

⁴Appeared in the arXiv on the same day with this article.

⁵The observed excess is also compatible with a spin-2 nature [2, 3, 4].

⁶We are working in a limit when interaction like $\kappa_W W_{\mu\nu}^a W_a^{\mu\nu}$, i.e., coupling between the SM $SU(2)$ gauge bosons and H_X vanishes.

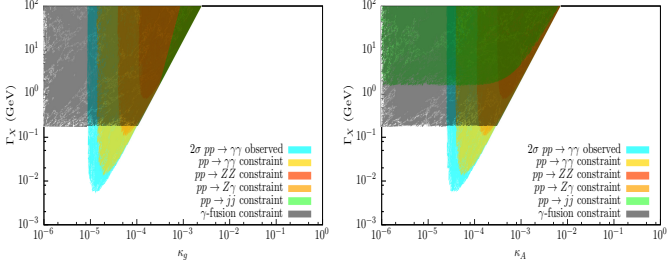


Figure 1: Variations of the Γ_X (in GeV) with κ_g (left) and κ_A (right). The details are explained in the text.

and H_X - γ - γ vertices are parametrised as κ_g and κ_A which encapsulate the effect of new physics appearing in the loops. The latter is an absolute necessity since SM-like couplings between the SM-gauge bosons and H_X appear inadequate [32] to explain the observed *sizable* decay width Γ_X [1, 3] and the production cross-section $\sigma(pp(gg) \rightarrow H_X \rightarrow \gamma\gamma) \sim O(10 \text{ fb})$ [1, 2, 3, 4], consistent with the results of various other LHC searches. The observations from different LHC searches put strong constraints on the κ_g - κ_A parameter space. The latter can be translated in terms of $H_X \rightarrow gg$, $H_X \rightarrow \gamma\gamma$ branching fractions (*Br*s) since they are $\propto 8\kappa_g^2$, $\kappa_A^2 \cos^4 \theta_W$, respectively. Moreover, the associated squared matrix elements are similar while the phase spaces are identical. The number ‘8’ appears from the colour factor and θ_W is the Weinberg angle [33].

After the electroweak symmetry breaking, the second term of eq. (1) generates effective interactions like $H_X \gamma \gamma$ and also $H_X Z \gamma$, $H_X ZZ$, even with vanishing κ_W . Their strengths are $\propto \kappa_A \cos^2 \theta_W$, $\kappa_A \sin \theta_W \cos \theta_W$ and $\kappa_A \sin^2 \theta_W$, respectively. It is thus, important to note that a non-zero $Br(H_X \rightarrow \gamma\gamma)$ would also imply non-zero $Br(H_X \rightarrow Z\gamma, ZZ)$ values since all of them are connected to κ_A . Their relative magnitudes, however, remain different depending on the factor of $\sin \theta_W$ or $\cos \theta_W$. Measurements from the experimental collaborations for the said processes, using 13 TeV data, remain yet inadequate⁷. Nevertheless, measured information for $H_X \rightarrow ZZ$, $Z\gamma$ and $H_X \rightarrow \gamma\gamma$ [38] processes from the 8 TeV searches definitely constrain the range of κ_A , κ_g parameters. For example, one obtains $\sigma(pp \rightarrow H_X \rightarrow ZZ) < 12 \text{ fb}$ [39] and $\sigma(pp \rightarrow H_X \rightarrow Z\gamma) < 11 \text{ fb}$ [40] from the similar searches performed by the ATLAS with 8 TeV data. The available parameter space is also constrained by the di-jets searches, given as $\sigma(pp \rightarrow jj) < 1.9 \text{ pb}$ [41]⁸, such that the missing evidence of $pp \rightarrow H_X \rightarrow jj$ process at the 13 TeV appears consistent. Needless to mention that the CMS collaboration has also made similar studies [44, 45, 46, 47]. Furthermore, if one wishes to account for a large Γ_X by introducing new, e.g., invisible decays, one needs to incorporate the constraints from monojet searches accordingly [48, 49].

In this article we have used the *expected* limits from 13 TeV LHC searches for ZZ , $Z\gamma$, jj and $\gamma\gamma$ processes, derived

using the 8 TeV results. We have used Madgraph v2.2.3 [50, 51] and observed that the production (via gluon fusion) cross-section with 13 TeV E_{CM} is roughly five times of the same with 8 TeV E_{CM} , i.e., $\sigma(pp \rightarrow H_X)|_{13 \text{ TeV}}/\sigma(pp \rightarrow H_X)|_{8 \text{ TeV}} \approx 5$, as also noted in Ref. [15]. Further, we have also used the constraint from Ref. [52] assuming that this resonance can also appear through photon fusion. In our numerical study we have used FeynRules 2.3 [53] to implement eq. (1) together with the SM Lagrangian. Subsequently, Madgraph v2.2.3 has been utilised to compute the production cross-section $\sigma(pp \rightarrow H_X)$ through gluon fusion and to calculate different partial decay widths of H_X . In this study we have utilised 3.2 fb^{-1} of ATLAS data at 13 TeV to accommodate the observed resonance. In detail, we have used ΔN , the discrepancy between the observed and expected number of events $= 13.6 \pm 3.69$. Further, for this purpose three 40 GeV bins are chosen for $690 \text{ GeV} \lesssim m_{\gamma\gamma}^{inv} \lesssim 810 \text{ GeV}$ [1] with an efficiency of 0.4 [2].

In order to study the effect of BSM physics, we first show the variation of Γ_X with changes in the new physics parameters, κ_g (left), κ_A (right), in Fig. 1. Here, we have varied κ_g , κ_A in the span of 10^{-6} - 1. In these two plots the cyan coloured region represents the allowed 2σ range of ΔN . The orange, golden and green coloured regions represent various zones in the Γ_X - κ_g (κ_A) planes that are excluded from the 8 TeV LHC measurements of $H_X \rightarrow ZZ$, $Z\gamma$, jj processes. The yellow coloured region remains excluded from the measurement of $H_X \rightarrow \gamma\gamma$ [38] process at the ATLAS with 8 TeV centre-of-mass energy. Lack of precision measurements for the latter, assuming $\sigma(pp \rightarrow H_X)|_{13 \text{ TeV}}/\sigma(pp \rightarrow H_X)|_{8 \text{ TeV}} \approx 5$, predicts a 2σ upper bound [6] on $\sigma(pp \rightarrow H_X \rightarrow \gamma\gamma)|_{13 \text{ TeV}}$ inconsistent with the one observed with 13 TeV. We will discuss this later in detail. Finally, the gray coloured region remains excluded from the photon fusion process, i.e., $\gamma\gamma \rightarrow H_X \rightarrow \gamma\gamma$, [52] which predicts a maximum for $Br(H_X \rightarrow \gamma\gamma)$, independent of $Br(H_X \rightarrow gg)$. The region excluded by the photon fusion process is estimated by assuming that H_X has only two decay modes gg , $\gamma\gamma$, i.e., $Br(H_X \rightarrow gg) + Br(H_X \rightarrow \gamma\gamma) = 1$. The observed limits on the *Br*s are subsequently translated in terms of κ_g and κ_A .

It is evident from Fig. 1 that expecting Γ_X as large as 45 GeV or more is perfectly consistent with the observed limits on ZZ , $\gamma\gamma$, $Z\gamma$ searches at the 8 TeV LHC. However, it is the di-jet searches which rules out the region of parameter space with $\Gamma_X > 3 \text{ GeV}$ (right plot), corresponding to $\kappa_g \gtrsim O(0.001)$ (left plot). The observed behaviour is well expected as $\Gamma_{H_X \rightarrow gg}$ and thus, Γ_X grows rapidly with κ_g compared to that with κ_A , i.e., $\Gamma_{H_X \rightarrow \gamma\gamma}$ since the latter is suppressed by a factor of $\cos^4 \theta_W/8$. For κ_A (estimated from $Br(H_X \rightarrow \gamma\gamma)$), the most stringent bound is coming from the photon fusion process which is represented by the gray coloured region. For the photon fusion process, $Br(H_X \rightarrow \gamma\gamma) \propto 1/\sqrt{\Gamma_X}$ [52] and thus, *smaller* upper bound on $Br(H_X \rightarrow \gamma\gamma)$ and hence, on κ_A is expected for larger Γ_X . This is evident from the right plot of Fig. 1. It is important to note that the photon fusion process can also provide an indirect bound on $Br(H_X \rightarrow gg)$, i.e., on κ_g , assuming $Br(H_X \rightarrow \gamma\gamma) + Br(H_X \rightarrow gg) = 1$. It is also apparent that

⁷The ATLAS and CMS collaborations have recently reported ZZ [34, 35] and $Z\gamma$ [36, 37] search results with early 13 TeV data.

⁸For di-jet searches, early 13 TeV results are also available [42, 43].

the photon fusion process discards $\Gamma_X \gtrsim 0.3$ GeV which is 10 times smaller than the one predicted from the di-jet search limit. Hence, given the observed large Γ_X from the ATLAS, one needs almost the *equal* amount of Γ_X from the hitherto unseen decay modes of this resonance, e.g., invisible decays. Here, we use $\Gamma_X = \Gamma_{H_X \rightarrow \gamma\gamma} + \Gamma_{H_X \rightarrow ZZ} + \Gamma_{H_X \rightarrow Z\gamma} + \Gamma_{H_X \rightarrow jj}$, as expected from eq. (1), to estimate $Br(H_X \rightarrow \gamma\gamma)$ for the photon fusion process [52]. It is now clear that in the chosen setup, no realistic values of κ_A , κ_g parameters can account for a total $\Gamma_X \gtrsim 0.3$ GeV. Thus, the presence of a *huge* additional decay width is essential for the studied construction which will be tightly constrained from the dark matter and monojet searches.

The discussion presented so far concerning the photon fusion process has one caveat related to the estimation of $Br(H_X \rightarrow gg)$. So far, we have used eq. (1) to estimate Γ_X , however, while evaluating the effect of photon fusion process on $Br(H_X \rightarrow gg)$, i.e., on κ_g (left plot of Fig. 1), we have used $Br(H_X \rightarrow \gamma\gamma) + Br(H_X \rightarrow gg) = 1$ which is *apparently* contradicting. At this point one must note that in the given construction the quantities $Br(H_X \rightarrow Z\gamma, ZZ)$, as already explained, are suppressed compared to $Br(H_X \rightarrow \gamma\gamma)$. Moreover, so far we have no information available for processes like $\gamma Z, ZZ \rightarrow H_X$. Thus, the assumption $Br(H_X \rightarrow gg) = 1 - Br(H_X \rightarrow \gamma\gamma)$ remains useful for estimating the scale of $Br(H_X \rightarrow gg)$. Using all the available branching fractions instead would yield *weaker* upper bounds on $Br(H_X \rightarrow gg)$, i.e., on κ_g .

It is evident from Fig. 1 that $\Gamma_X \gtrsim 0.3$ GeV appears excluded from the relevant existing LHC limits and from the constraint of photon fusion process. This observation demands the existence of *huge* additional decay width to reach the target of 45 GeV. If we call this additional width as Γ_X^{add} , without specifying the origin, then one can write $\Gamma_X^{tot} \equiv \Gamma_X = \Gamma_{H_X \rightarrow \gamma\gamma} + \Gamma_{H_X \rightarrow ZZ} + \Gamma_{H_X \rightarrow Z\gamma} + \Gamma_{H_X \rightarrow jj} + \Gamma_X^{add}$. This approach will modify all the associated branching ratios as will be explored subsequently by *choosing* three different values of the total decay widths: (1) 1 GeV (small width), (2) 10 GeV (moderate width) and (3) 45 GeV (large width).

The subsequent effects of the aforesaid construction are explored in Fig. 2 where we have investigated the impact of diverse LHC and photon fusion constraints in the $Br(H_X \rightarrow gg)$ - $Br(H_X \rightarrow \gamma\gamma)$ plane. These two Br s are expected to show *some kind* of correlation⁹ between them since the observed excess appears through $gg \rightarrow H_X$ process followed by $H_X \rightarrow \gamma\gamma$ decay. It is also possible to observe a similar correlation in the κ_g , κ_A plane since $Br(H_X \rightarrow gg)$, $Br(H_X \rightarrow \gamma\gamma) \propto \kappa_g^2$, κ_A^2 , respectively. In Fig. 2 the black coloured line represents the best-fit value corresponding to $\Delta N = 13.6$ while the cyan and blue coloured bands represent the 1σ ($9.91 \lesssim \Delta N \lesssim 17.29$) and 2σ ($6.22 \lesssim \Delta N \lesssim 20.98$) allowed regions in the concerned planes, respectively. The orange, golden, green and yellow coloured regions, similar to Fig. 1, represent various zones in the concerned plane that are excluded from 8 TeV LHC limits on $H_X \rightarrow ZZ, Z\gamma, jj$ and $\gamma\gamma$ processes. In the case of $H_X \rightarrow \gamma\gamma$ process, assuming $\sigma(pp \rightarrow H_X)|_{13 \text{ TeV}}/\sigma(pp \rightarrow H_X)|_{8 \text{ TeV}} \approx 5$,

one would expect a 2σ upper bound [6] on $\sigma(pp \rightarrow H_X \rightarrow \gamma\gamma)|_{13 \text{ TeV}}$ as 10 fb using the ATLAS data. This is in tension with the 13 TeV ATLAS observation [1] and rules out higher values of the observed $\sigma(pp \rightarrow H_X \rightarrow \gamma\gamma)$, starting from the central one. A similar analysis using the CMS data [5] excludes the higher values of the observed $\sigma(pp \rightarrow H_X \rightarrow \gamma\gamma)|_{13 \text{ TeV}}$ [2] beyond 1σ .

Lastly, the photon fusion process at the LHC, which predicts a maximum for $Br(H_X \rightarrow \gamma\gamma)$ independent of $Br(H_X \rightarrow gg)$, rules out the gray coloured region in the $Br(H_X \rightarrow gg)$ - $Br(H_X \rightarrow \gamma\gamma)$ plane. It is interesting to note that the constraint for the photon fusion was derived with the assumption of $Br(H_X \rightarrow gg) + Br(H_X \rightarrow \gamma\gamma) = 1$ which discards a region where $Br(H_X \rightarrow gg) + Br(H_X \rightarrow \gamma\gamma) > 1$. For the three chosen values of Γ_X , the maximum $Br(H_X \rightarrow \gamma\gamma)$ is estimated [52] as $\sim 0.42, 0.13, 0.06$, respectively and thus, the regions with $Br(H_X \rightarrow gg) > 0.58$ (left plot of Fig. 2), $Br(H_X \rightarrow gg) > 0.87$ (middle plot of Fig. 2), $Br(H_X \rightarrow gg) > 0.94$ (right plot of Fig. 2) remain ruled out. The upper limits of $Br(H_X \rightarrow gg)$, as depicted in Fig. 2 are purely illustrative. This is because, following our earlier discussion, $Br(H_X \rightarrow gg) = 1 - Br(H_X \rightarrow \gamma\gamma)$ estimated in a regime when $\Gamma_X^{add} \approx \Gamma_X^{tot} \equiv \Gamma_X$ appears simply illustrative. For the rest of the processes the primary productions are driven by the gluon fusion process. The latter gives a high value for $Br(H_X \rightarrow gg)$ with increasing κ_g and as a consequence remains excluded from the di-jet search limits, especially for moderate to large Γ_X . For example, for the choice of $\Gamma_X = 10$ GeV one gets $Br(H_X \rightarrow gg)_{max} \sim 0.40$ (middle plot of Fig. 2) while for the choice of $\Gamma_X = 45$ GeV one ends up with $Br(H_X \rightarrow gg)_{max} \sim 0.20$ (right plot of Fig. 2). In the case of small decay width (left plot of Fig. 2) constraint from the di-jet searches remains ineffectual.

It is evident from eq. (1) that $Br(H_X \rightarrow ZZ)$, $Br(H_X \rightarrow Z\gamma)$ are suppressed compared to $Br(H_X \rightarrow \gamma\gamma)$ by factors of $\tan^4 \theta_W$ and $\tan^2 \theta_W$ (numerically ~ 0.09 and 0.3), respectively which is also apparent from Fig. 2. Thus, unless one introduces interaction like $\kappa_W W_{\mu\nu}^a W_a^{\mu\nu}$ ($W_{\mu\nu}^a$ as the $SU(2)$ field strengths) these modes remain sub-leading. One can, nevertheless, compensate these deficits with a larger $Br(H_X \rightarrow gg)$, assuming $gg \rightarrow H_X$ to be the leading production channel. These behaviours are reflected in Fig. 2 where the regions excluded from ZZ and $Z\gamma$ searches appear with lateral shifts towards larger $Br(H_X \rightarrow gg)$ values compared to $Br(H_X \rightarrow \gamma\gamma)$ values, required to reproduce the observed excess. Larger $Br(H_X \rightarrow gg)$ and hence larger Γ_X appear naturally for higher κ_g values which are in tension with the di-jet searches. Increasing κ_A receives constraint from the photon fusion process. The ZZ and $Z\gamma$ constraints, as already mentioned, require large values for both of the $Br(H_X \rightarrow gg)$ and $Br(H_X \rightarrow \gamma\gamma)$. The former faces tension from the di-jet search limits (moderate and large Γ_X scenarios) while the latter, if not excluded by the photon fusion constraint, might give larger ΔN than actually observed. Hence, the parameter space ruled out by these constraints do not affect the signal region compatible for explaining the observed excess. The key feature of Fig. 2 is the prediction

⁹This correlation may disappear if this new resonance arises through the photon fusion process [52].

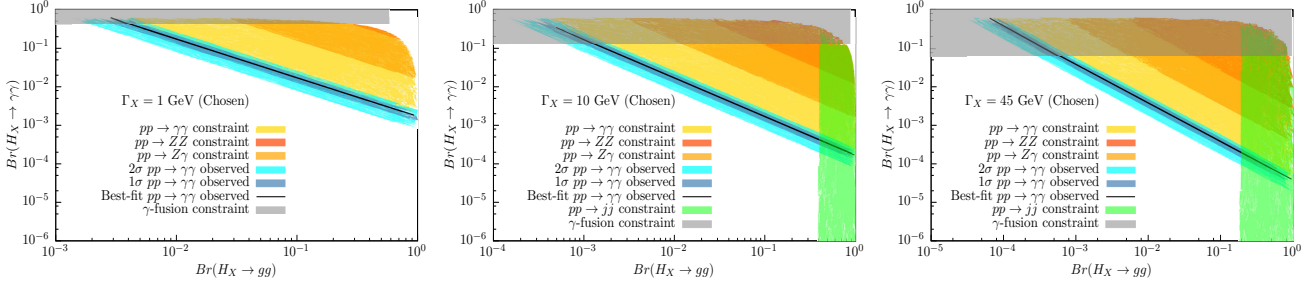


Figure 2: Correlations in the $Br(H_X \rightarrow gg) - Br(H_X \rightarrow \gamma\gamma)$ plane for the three different choices of Γ_X : 1 GeV (left), 10 GeV (middle), and 45 GeV (right) compatible with the observed $\sigma(pp \rightarrow H_X \rightarrow \gamma\gamma)$. The details are explained in the text.

of the value of product¹⁰ $Br(H_X \rightarrow gg) \times Br(H_X \rightarrow \gamma\gamma)$ (henceforth written as $Br^2(\gamma\gamma \times gg)$). From the best-fit line we observe that this value changes from $O(10^{-3})$ to $O(10^{-5})$ as the chosen Γ_X changes from 1 GeV to 45 GeV. Explicitly, $0.08(1.73) \times 10^{-3(5)} \lesssim Br^2(\gamma\gamma \times gg) \lesssim 1.93(4.28) \times 10^{-3(5)}$ for $\Gamma_X = 1(45)$ GeV using 2σ limits on ΔN . We will use these information subsequently.

Now we are ready to discuss the presence of other BSM particles that are essential to explain this excess through higher order processes. Information about these states are encapsulated within κ_g, κ_A (see eq. (1)). These states must not be very heavy to avoid propagator suppression and at the same time, must possess sizable couplings with H_X to reproduce the detected excess. Concerning the leading production, i.e., $gg \rightarrow H_X$, the possible candidate(s) is(are) either new coloured scalar(s) Φ or additional coloured fermion(s) F , possibly vector-like. These new particles must simultaneously couple to gluons as well as to H_X and, are possibly embedded in a representation of some larger symmetry group. If these new scalars/fermions are also responsible for producing an enhanced $Br(H_X \rightarrow \gamma\gamma)$, they must carry electrical charges to get coupled to a photon. However, the other non-minimal possibility is to consider another set of uncoloured but electrically charged fermion(s), scalar(s) or gauge boson(s) (appears in theories with extended non-Abelian gauge sector). Note that contributions from new chiral fermions produce a destructive effect compared to the bosonic contributions and thus, often are not compatible with the observed excess. On the other hand, vector-like fermions remain a viable alternative. The presence of an extended scalar sector has additional phenomenological advantages, e.g., stability of the SM-Higgs potential up to the Planck scale [55, 56, 57, 58]. This argument also holds true for new gauge boson(s). We, however, do not consider them in this article since they are hinted to be rather heavy $\gtrsim 2.5$ TeV [59, 60]. In a nutshell, we conclude that to accommodate the observed di-photon excess one needs sizable couplings between H_X and the new particles, for which coloured and/or electrically charged scalars or fermions remain the realistic options. Moreover, in the presence of the said new states, an enhanced $Br(H_X \rightarrow \gamma\gamma)$ is more anticipated compared to an enlarged $Br(H_X \rightarrow gg)$ as for the latter experimental evidences are still missing.

In the presence of a new BSM scalar Φ , with mass M_Φ , electric charge Q_Φ (in the units of $|e|$) and number of colour N_Φ^c , the $Br(H_X \rightarrow \gamma\gamma)$ can be written as [32, 61]:

$$Br(H_X \rightarrow \gamma\gamma) = \frac{\alpha^2 M_X^3}{1024\pi^3 \Gamma_X} \left| \frac{g_{\Phi\Phi H_X}}{M_\Phi^2} N_\Phi^c Q_\Phi^2 A_\Phi(x_\Phi) \right|^2. \quad (2)$$

Here, α_{em} is the electromagnetic coupling constant, $g_{\Phi\Phi H_X}$ represents the coupling between Φ and H_X and the detail of $A_\Phi(x_\Phi)$ function, where $x_\Phi = 4M_\Phi^2/M_X^2$, is given in Ref. [32]. Keeping in mind the issue of perturbativity we choose $-\sqrt{4\pi} \lesssim g_{\Phi\Phi H_X} \lesssim \sqrt{4\pi}$, in our numerical analyses. The quantity $g_{\Phi\Phi H_X}$ parametrises the information about the vacuum expectation value (VEV) of H_X and the amount of possible mixing between H_X and the SM-Higgs. From eq. (2) it appears that a larger $g_{\Phi\Phi H_X}$ is useful to produce a bigger $Br(H_X \rightarrow \gamma\gamma)$. In reality, however, such scenarios are unrealistic as they correspond to either experimentally challenging large mixing within H_X and the SM-Higgs or a large VEV for H_X inconsistent with the electroweak precision tests [33].

It is apparent from eq. (2) that depending on the values of M_Φ, Q_Φ and N_Φ^c , the quantity $Br(H_X \rightarrow \gamma\gamma)$ can receive sizable enhancement. An enlargement is also possible if the future LHC observation confirms a smaller Γ_X . In our numerical analyses we choose $400 \text{ GeV} \lesssim M_\Phi \lesssim 1000 \text{ GeV}$, consistent with the existing collider bounds on such exotic particles [62, 63, 64]. A sample variation of $Br(H_X \rightarrow \gamma\gamma)$ in the $M_\Phi - g_{\Phi\Phi H_X}$ plane for a colour singlet ($N_\Phi^c = 1$), triply charged ($Q_\Phi = 3$), scalar with different Γ_X , 1 GeV (left) and 45 GeV (right) is shown in Fig. 3. It is evident from Fig. 3 that an experimentally viable light, i.e., $M_\Phi = 400 \text{ GeV}$, colour singlet Φ with $Q_\Phi = 3$ can produce at most a $Br(H_X \rightarrow \gamma\gamma) \sim O(10^{-8})$ (left plot) when Γ_X is small, i.e., 1 GeV. Choosing $\Gamma_X = 45 \text{ GeV}$ instead one faces a reduction by a factor of 45 (right plot). From eq. (2) we see that $Br(H_X \rightarrow \gamma\gamma) \propto Q_\Phi^4$. Thus, even for an exotic colour singlet Φ with $Q_\Phi = 10$, one would expect a maximum $Br(H_X \rightarrow \gamma\gamma) \sim O(10^{-6})$ keeping $\Gamma_X, M_\Phi = 1 \text{ GeV}, 400 \text{ GeV}$. Now, from our previous discussion in the context of Fig. 2, we have estimated $Br^2(\gamma\gamma \times gg)$ as $\sim O(10^{-3})$ and $\sim O(10^{-5})$ for the choice of $\Gamma_X = 1$ and 45 GeV, respectively from the best-fit value of ΔN . Hence, the maximum $Br(H_X \rightarrow \gamma\gamma)$, extracted from Fig. 3 using eq. (2) for a 400 GeV Φ with $N_\Phi^c, Q_\Phi = 1, 10$, would give an *unrealistic* $Br(H_X \rightarrow gg) \sim 400(180)$ for $\Gamma_X = 1(45)$ GeV scenarios. One may try to consider a *similar* but *coloured* (say

¹⁰The fact that the same product is $\sim O(10^{-11})$ [54] for a 750 GeV state with SM-like properties justifies BSM nature of this excess.

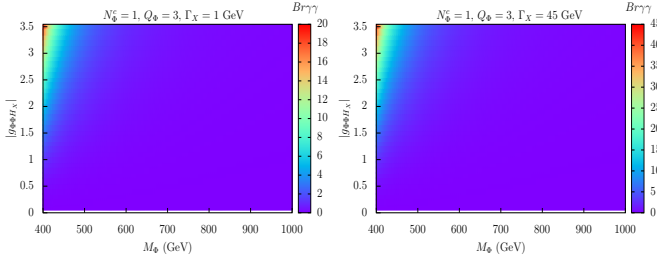


Figure 3: Plots showing the variation of $Br\gamma\gamma = Br(H_X \rightarrow \gamma\gamma) \times 10^n$ in the $M_\Phi - |g_{\Phi H_X}|$ plane for $N_\Phi^c, Q_\Phi = 1, 3$ with $\Gamma_X = 1$ GeV (left) and 45 GeV (right). The chosen ranges for M_Φ and $g_{\Phi H_X}$ are explained in the text. The multiplicative factor $n = 9(11)$ for $\Gamma_X = 1(45)$ GeV.

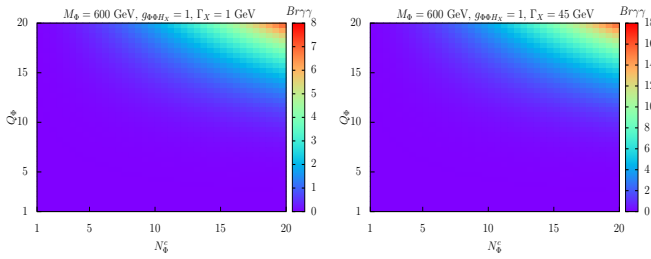


Figure 4: Variation of $Br\gamma\gamma = Br(H_X \rightarrow \gamma\gamma) \times 10^n$ in the $N_\Phi^c - Q_\Phi$ plane for $M_\Phi = 600$ GeV, $g_{\Phi H_X} = 1$, $\Gamma_X = 1$ GeV (left) and 45 GeV (right). Here, $n = 5(7)$ for $\Gamma_X = 1(45)$ GeV.

$N_\Phi^c = 3$) Φ which predicts a maximum $Br(H_X \rightarrow \gamma\gamma) \sim \mathcal{O}(10^{-5})$ for $\Gamma_X = 1$ GeV. However, one still needs an *unrealistic* $Br(H_X \rightarrow gg) \sim 50$ in this scenario. Moreover, for a Φ with non-zero colours one must carefully investigate the $H_X \rightarrow jj$ constraint, even for a realistic $Br(H_X \rightarrow gg)$, especially for moderate to large Γ_X .

From the last discussion it appears that the use of new BSM scalar is not adequate to explain the observed excess. In order to explore this further we have plotted the change of $Br(H_X \rightarrow \gamma\gamma)$ in the $N_\Phi^c - Q_\Phi$ plane in Fig. 4 with $M_\Phi, g_{\Phi H_X} = 600$ GeV, 1 for the choice of $\Gamma_X = 1$ GeV (left) and 45 GeV (right). Here, we vary both N_Φ^c, Q_Φ in the range of 1 : 20 and the chosen values of $M_\Phi, g_{\Phi H_X}$ are purely illustrative. It is apparent from both of these plots that to satisfy $Br^2(\gamma\gamma \times gg)$, consistent with the observation of Fig. 2, one should have an *unrealistic* $Br(H_X \rightarrow gg) \sim 10(5)$ for $\Gamma_X = 1(45)$ GeV. Adopting smaller M_Φ (say 400 GeV) simultaneously with a larger $g_{\Phi H_X}$ (say ± 3) one can reach a maximum $Br(H_X \rightarrow \gamma\gamma) \sim 0.012$ and ~ 0.00025 for $\Gamma_X = 1$ and 45 GeV, respectively considering $N_\Phi^c \gtrsim 14, Q_\Phi \gtrsim 16$. Here, we have used eq. (2) and information from Fig. 4. So, apparently these exotic scenarios can give a *realistic* $Br(H_X \rightarrow gg) \lesssim \mathcal{O}(0.1)$, consistent with the di-jet searches (see Fig. 2). However, this moderate $Br(H_X \rightarrow gg)$ value may get excluded from the future LHC searches with expected higher sensitivity. Moreover, one must carefully re-evaluate the maximum value for $g_{\Phi H_X}$ in a consistent theory framework. It is now evident from the last discussion that the

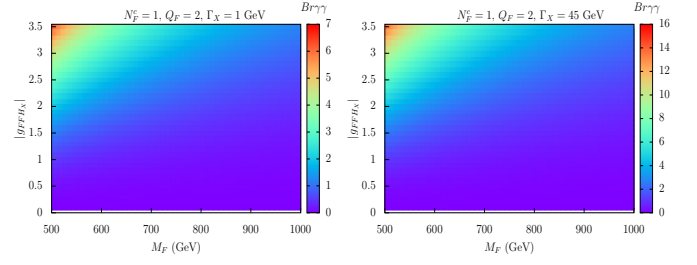


Figure 5: Plots showing the variation of $Br\gamma\gamma = Br(H_X \rightarrow \gamma\gamma) \times 10^n$ in the $M_F - |g_{FFH_X}|$ plane for $N_F^c, Q_F = 1, 2$ with $\Gamma_X = 1$ GeV (left) and 45 GeV (right). The chosen ranges for M_F and g_{FFH_X} are explained in the text. Here, $n = 3(5)$ for the left(right) plot.

presence of BSM Φ s, instrumental to reproduce the observed excess, requires really high electric and colour charges. Particles with such high colour charges are expected to be produced amply at the LHC, unless very massive and hence, rather stringent constraints are expected on their existence. We thus, leave our discussion about the BSM scalars without further detail. We note in passing that Q_Φ value as high as 20 can be interpreted as an effective electric charge, keeping N_Φ^c fixed. For example data-set with $Q_\Phi = 20$ for a fixed N_Φ^c , using eq. (2), can be thought of as a coloured/uncoloured multiplet with members of *almost the same* masses and having electric charges from ± 1 to ± 10 .

Let us now investigate a similar scenario in the presence of new BSM vector-like fermion, F . For a fermion with mass M_F , electric charge Q_F (in the units of $|e|$), number of colours N_F^c , the quantity $Br(H_X \rightarrow \gamma\gamma)$ is expressed as [32, 61]:

$$Br(H_X \rightarrow \gamma\gamma) = \frac{\alpha^2 M_X^3}{1024\pi^3 \Gamma_X} \left| \frac{2g_{FFH_X}}{M_F} N_F^c Q_F^2 A_F(x_F) \right|^2. \quad (3)$$

Here, g_{FFH_X} represents the generic coupling between F and H_X . The function $A_F(x_F)$, with $x_F = 4M_F^2/M_X^2$, is given in Ref. [32]. We consider $500 \text{ GeV} \lesssim M_F \lesssim 1 \text{ TeV}$ (see Ref. [65] and references therein) while g_{FFH_X} is varied in a range similar to $g_{\Phi H_X}$, based on the same argument.

The sample variation of $Br(H_X \rightarrow \gamma\gamma)$ in the $M_F - g_{FFH_X}$ plane for a colour singlet doubly charged ($Q_F = 2$) fermion is shown in Fig. 5 for $\Gamma_X = 1$ (left) and 45 GeV (right). It is easy to see from these plots that the presence of BSM fermions is more efficient to raise $Br(H_X \rightarrow \gamma\gamma)$ compared to the BSM scalars. For example a colour singlet doubly charged fermion can produce $Br(H_X \rightarrow \gamma\gamma)$ as high as 0.007 and $\sim 10^{-4}$ for $\Gamma_X = 1$ and 45 GeV, respectively. These numbers are orders of magnitude larger compared to the same from Fig. 3 and, as stated before, can only be achieved for a Φ with very high Q_Φ and N_Φ^c . These enhanced $Br(H_X \rightarrow \gamma\gamma)$ values are also useful to estimate *realistic* values of $Br(H_X \rightarrow gg)$, using the information from Fig. 2. As an example, from Fig. 5, with the maximum of $Br(H_X \rightarrow \gamma\gamma)$, one can estimate $Br(H_X \rightarrow gg) \sim 0.14(0.063)$ for $\Gamma_X = 1(45)$ GeV using the derived bound on $Br^2(\gamma\gamma \times gg)$. Clearly, one can easily reproduce the observed excess, especially for smaller Γ_X , without any difficulty. However, for larger Γ_X , depending on its value, some of the $Br(H_X \rightarrow gg)$ values

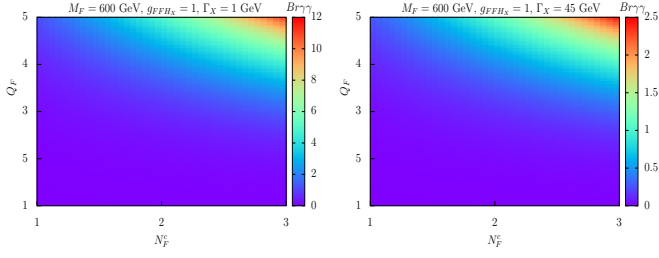


Figure 6: Variation of $Br\gamma\gamma\gamma = Br(H_X \rightarrow \gamma\gamma) \times 10^n$ in the $N_F^c - Q_F$ plane for $M_F = 600$ GeV, $g_{FFH_X} = 1$, $\Gamma_X = 1$ GeV (left) and 45 GeV (right). For the left(right) plot $n = 2(3)$.

remain excluded from the di-jet searches as already depicted in Fig. 2.

In order to study the behaviour of $Br(H_X \rightarrow \gamma\gamma)$ with changes in the $N_F^c - Q_F$ values we have plotted the same in Fig. 6 for the choice of $\Gamma_X = 1$ GeV (left) and 45 GeV (right). The chosen M_F, g_{FFH_X} values are purely illustrative. We vary $N_F^c(Q_F)$ in the range of 1 : 3(5). It is visible from these plots that an electrically charged coloured fermion can generate $Br(H_X \rightarrow \gamma\gamma)$ as high as 0.12(0.0025) for $\Gamma_X = 1(45)$ GeV. Using the information from Fig. 6 and our knowledge of Fig. 2, these numbers predict $0.01(0.004) \lesssim Br(H_X \rightarrow gg) \lesssim 0.1(0.05)$ for $\Gamma_X = 1(45)$ GeV. These numbers are absolutely consistent with the di-jet searches as shown in Fig. 2. For exotic fermions a lower value of M_F (say 400 GeV) and a higher g_{FFH_X} value (say $\pm\sqrt{4\pi}$), especially for small Γ_X , will produce $Br(H_X \rightarrow \gamma\gamma)$ either > 1 or inconsistent with the constraint of photon fusion process for certain region of the $N_F^c - Q_F$ plane, e.g., $1 \lesssim N_F^c \lesssim 3, Q_F > 3$. Further, compared to the BSM scalars, the BSM fermions can appear instrumental to reproduce the observed excess with realistic values of $Br(H_X \rightarrow gg)$ and $Br(H_X \rightarrow \gamma\gamma)$ even with $M_F = 1$ TeV. As for the latter with $g_{FFH_X} = 1, \Gamma_X = 45$ GeV and with $1 \lesssim N_F^c(Q_F) \lesssim 3(5)$ one gets $0.0001 \lesssim Br(H_X \rightarrow \gamma\gamma) \lesssim 0.0008$ and thus, $0.0125 \lesssim Br(H_X \rightarrow gg) \lesssim 0.1$, consistent with Fig. 2. We note in passing that, similar to the scalars, one can also explain Fig. 6, say $N_F^c, Q_F = 1, 4$, with a single uncoloured multiplet with quasi-degenerate masses for the members and Q_F ranging from ± 1 to ± 3 .

The proficiency of the BSM fermions over the scalars are now established. Although one can reproduce the excess with a colour singlet fermion with high Q_F (see Fig. 6), nevertheless, it is an absolute necessity to explore the scenario with $N_F^c > 1$ as otherwise the expected BSM origin for $gg \rightarrow H_X$ process remains unexplained. This scenario may receive constraint from di-jet searches provided the enhanced efficiency expected from the future LHC operation.

The exotic fermions, similar to $Br(H_X \rightarrow \gamma\gamma)$ (see eq. (3)), can also contribute to $Br(H_X \rightarrow gg)$. At the leading order this branching ratio [66] is given as:

$$Br(H_X \rightarrow gg) = \frac{\alpha_s^2 M_X^3}{512\pi^3 \Gamma_X} \left| \frac{2g_{FFH_X}}{M_F} A_F(x_F) \right|^2. \quad (4)$$

Here, α_s is the strong coupling constant. In our numerical anal-

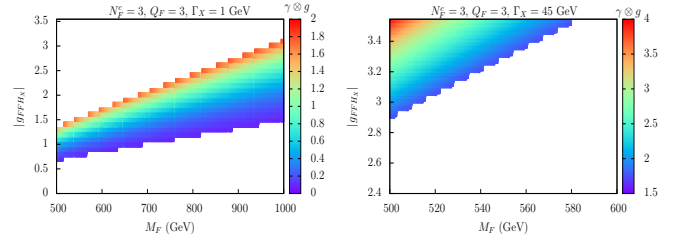


Figure 7: Plots showing the variation of $\gamma \otimes g \equiv Br(H_X \rightarrow \gamma\gamma) \times Br(H_X \rightarrow gg) \times 10^n$ in the $M_F - |g_{FFH_X}|$ plane for $N_F^c = 3, Q_F = 3$ with $\Gamma_X = 1$ GeV (left) and 45 GeV (right). Here, $n = 3(5)$ for $\Gamma_X = 1(45)$ GeV.

ysis we have multiplied $Br(H_X \rightarrow gg)$, as shown in eq. (4), by a factor of 1.5, relevant for the higher order effects of strong interactions. Using eqs. (3) and (4) simultaneously we have studied a sample variation of $Br^2(\gamma\gamma \times gg)$ in the $M_F - g_{FFH_X}$ plane as shown by Fig. 7 with $\Gamma_X = 1$ GeV (left) and 45 GeV (right). For this figure M_F, g_{FFH_X} are varied as of Fig. 5 and we work with $N_F^c = 3$ and $Q_F = 3$. The observed behaviours of $Br^2(\gamma\gamma \times gg)$ with different parameters, i.e., M_F, g_{FFH_X} and Γ_X are expected from eqs. (3) and (4). For example, both $Br(H_X \rightarrow \gamma\gamma)$ and $Br(H_X \rightarrow gg)$ are $\propto \Gamma_X^{-1}$ and thus, shrinking of the allowed parameter space, compatible with the observed excess, for larger Γ_X , 45 GeV, (right plot of Fig. 7) is anticipated. At the same time, these two branching ratios are $\propto g_{FFH_X}^2/M_F^2$ (see eqs. (3), (4)). Hence, apparent lowering of $Br^2(\gamma\gamma \times gg)$ for larger M_F values must be compensated with larger g_{FFH_X} values in order to remain compatible with the excess. This feature is depicted in Fig. 7, notably for the left one. The most useful aspect of Fig. 7 is connected with the estimation of future detection possibility for the process $gg \rightarrow H_X^* \rightarrow F\bar{F}$. Assuming that the future measurements indicate a narrow width for this excess, say 1 GeV, then the room for measuring $\sigma(gg \rightarrow H_X^* \rightarrow F\bar{F})$ is less promising for two reasons: (1). The expected enhancement in the production for low M_F region is ameliorated with a relatively small g_{FFH_X} and (2). In the high g_{FFH_X} regime, the same logic remains applicable through heavier M_F . These two features are visible from the left plot of Fig. 7. On the contrary, a more stringent limit, i.e., $Br^2(\gamma\gamma \times gg) \sim O(10^{-5})$, for larger $\Gamma_X = 45$ GeV prefers smaller M_F and larger g_{FFH_X} (see right plot of Fig. 7). Both of these would appear useful to enhance $\sigma(gg \rightarrow H_X^* \rightarrow F\bar{F})$.

Conclusions: To summarise, the LHC run-II has already observed an excess in the di-photon invariant mass distribution near 750 GeV. This excess, as argued in this article, definitely requires BSM physics. In this article we tried to explore this excess, assuming a spin-0 nature, using an simplified effective Lagrangian, sensitive to *new* physics effects. The chosen framework helped us to estimate a lower bound of Γ_X , consistent with the different LHC constraints and photon fusion process, for changes in the new physics parameters, κ_g, κ_A . We have also explored the possible correlation between $Br(H_X \rightarrow \gamma\gamma)$ and $Br(H_X \rightarrow gg)$ in the light of the observed excess

and diverse possible constraints. This correlation provides a *model-independent but Γ_X -dependent* bound on $Br(H_X \rightarrow \gamma\gamma) \times Br(H_X \rightarrow gg)$. Subsequently, we have utilised this correlation to scrutinise the effect of other BSM scalars, fermions with various electric charge, number of colour which simultaneously couple to H_X and gg , $\gamma\gamma$ and might appear instrumental to reproduce this excess through higher order processes. Our analyses show that to accommodate the observed excess, the presence of additional BSM fermions are preferred compared to the scalars. Moreover, detecting these new fermions in the future is more anticipated for a large width of the observed excess. In conclusion, given this di-photon excess survives with more data-set, this can not be an isolated *surprise*. Rather, this must be the pioneering evidence of a BSM mass spectrum while other heavier members are awaiting to be detected.

Acknowledgments

The work of JC is supported by the Department of Science and Technology, Government of India under the Grant Agreement number IFA12-PH-34 (INSPIRE Faculty Award). The work of AC is supported by the Lancaster-Manchester-Sheffield Consortium for Fundamental Physics under STFC Grant No. ST/L000520/1. PG acknowledges the support from P2IO Excellence Laboratory (LABEX). The work of SM is partially supported by funding available from the Department of Atomic Energy, Government of India, for the Regional Centre for Accelerator-based Particle Physics (RECAPP), Harish-Chandra Research Institute.

References

- [1] Search for resonances decaying to photon pairs in 3.2 fb^{-1} of pp collisions at $\sqrt{s} = 13 \text{ TeV}$ with the ATLAS detector (2015). ATLAS-CONF-2015-081.
- [2] Search for new physics in high mass diphoton events in proton-proton collisions at 13 TeV (2015). CMS-PAS-EXO-15-004.
- [3] Search for resonances in diphoton events with the ATLAS detector at $\sqrt{s} = 13 \text{ TeV}$ (2016). ATLAS-CONF-2016-018.
- [4] Search for new physics in high mass diphoton events in 3.3 fb^{-1} of proton-proton collisions at $\sqrt{s} = 13 \text{ TeV}$ and combined interpretation of searches at 8 TeV and 13 TeV (2016). CMS-PAS-EXO-16-018.
- [5] Search for High-Mass Diphoton Resonances in pp Collisions at $\sqrt{s} = 8 \text{ TeV}$ with the CMS Detector (2015). CMS-PAS-EXO-12-045.
- [6] G. Aad, et al., Search for high-mass diphoton resonances in pp collisions at $\sqrt{s} = 8 \text{ TeV}$ with the ATLAS detector, Phys. Rev. D92 (2015) 032004.
- [7] K. Harigaya, Y. Nomura, Composite Models for the 750 GeV Diphoton Excess, Phys. Lett. B754 (2016) 151–156.
- [8] Y. Mambrini, G. Arcadi, A. Djouadi, The LHC diphoton resonance and dark matter, Phys. Lett. B755 (2016) 426–432.
- [9] M. Backovic, A. Mariotti, D. Redigolo, Di-photon excess illuminates Dark Matter, JHEP 03 (2016) 157.
- [10] A. Angelescu, A. Djouadi, G. Moreau, Scenarii for interpretations of the LHC diphoton excess: two Higgs doublets and vector-like quarks and leptons, Phys. Lett. B756 (2016) 126–132.
- [11] Y. Nakai, R. Sato, K. Tobioka, Footprints of New Strong Dynamics via Anomaly and the 750 GeV Diphoton, Phys. Rev. Lett. 116 (2016) 151802.
- [12] S. Knapen, T. Melia, M. Papucci, K. Zurek, Rays of light from the LHC, Phys. Rev. D93 (2016) 075020.
- [13] D. Buttazzo, A. Greljo, D. Marzocca, Knocking on new physics door with a scalar resonance, Eur. Phys. J. C76 (2016) 116.
- [14] A. Pilaftsis, Diphoton Signatures from Heavy Axion Decays at the CERN Large Hadron Collider, Phys. Rev. D93 (2016) 015017.
- [15] R. Franceschini, G. F. Giudice, J. F. Kamenik, M. McCullough, A. Pomarol, R. Rattazzi, M. Redi, F. Riva, A. Strumia, R. Torre, What is the $\gamma\gamma$ resonance at 750 GeV?, JHEP 03 (2016) 144.
- [16] S. Di Chiara, L. Marzola, M. Raidal, First interpretation of the 750 GeV diphoton resonance at the LHC, Phys. Rev. D93 (2016) 095018.
- [17] T. Higaki, K. S. Jeong, N. Kitajima, F. Takahashi, The QCD Axion from Aligned Axions and Diphoton Excess, Phys. Lett. B755 (2016) 13–16.
- [18] S. D. McDermott, P. Meade, H. Ramani, Singlet Scalar Resonances and the Diphoton Excess, Phys. Lett. B755 (2016) 353–357.
- [19] J. Ellis, S. A. R. Ellis, J. Quevillon, V. Sanz, T. You, On the Interpretation of a Possible $\sim 750 \text{ GeV}$ Particle Decaying into $\gamma\gamma$, JHEP 03 (2016) 176.
- [20] M. Low, A. Tesi, L.-T. Wang, A pseudoscalar decaying to photon pairs in the early LHC Run 2 data, JHEP 03 (2016) 108.
- [21] B. Bellazzini, R. Franceschini, F. Sala, J. Serra, Goldstones in Diphotons, JHEP 04 (2016) 072.
- [22] R. S. Gupta, S. Jger, Y. Kats, G. Perez, E. Stamou, Interpreting a 750 GeV Diphoton Resonance (2015).
- [23] C. Petersson, R. Torre, 750 GeV Diphoton Excess from the Goldstino Superpartner, Phys. Rev. Lett. 116 (2016) 151804.
- [24] E. Molinaro, F. Sannino, N. Vignaroli, Minimal Composite Dynamics versus Axion Origin of the Diphoton excess (2015).
- [25] W. Chao, R. Huo, J.-H. Yu, The Minimal Scalar-Stealth Top Interpretation of the Diphoton Excess (2015).
- [26] Q.-H. Cao, Y. Liu, K.-P. Xie, B. Yan, D.-M. Zhang, A Boost Test of Anomalous Diphoton Resonance at the LHC (2015).
- [27] A. Kobakhidze, F. Wang, L. Wu, J. M. Yang, M. Zhang, 750 GeV diphoton resonance in a top and bottom seesaw model, Phys. Lett. B757 (2016) 92–96.
- [28] D. Curtin, C. B. Verhaaren, Quirky Explanations for the Diphoton Excess, Phys. Rev. D93 (2016) 055011.
- [29] A. Ahmed, B. M. Dillon, B. Grzadkowski, J. F. Gunion, Y. Jiang, Higgs-radion interpretation of 750 GeV di-photon excess at the LHC (2015).
- [30] L. D. Landau, On the angular momentum of a system of two photons, Dokl. Akad. Nauk Ser. Fiz. 60 (1948) 207–209.
- [31] C.-N. Yang, Selection Rules for the Dematerialization of a Particle Into Two Photons, Phys. Rev. 77 (1950) 242–245.
- [32] M. Carena, I. Low, C. E. M. Wagner, Implications of a Modified Higgs to Diphoton Decay Width, JHEP 08 (2012) 060.
- [33] K. A. Olive, et al., Review of Particle Physics, Chin. Phys. C38 (2014) 090001.
- [34] Search for high-mass resonances decaying into a Z boson pair in the $\ell\ell\nu\nu$ final state in pp collisions at $\sqrt{s} = 13 \text{ TeV}$ with the ATLAS detector (2016). ATLAS-CONF-2016-012.
- [35] Measurement of the ZZ production cross section and $Z \rightarrow \ell\ell'\ell'\ell'$ branching fraction in pp collisions at $\sqrt{s} = 13 \text{ TeV}$ (2016). CMS-PAS-SMP-16-001.
- [36] T. A. collaboration, Search for heavy resonances decaying to a Z boson and a photon in pp collisions at $\sqrt{s} = 13 \text{ TeV}$ with the ATLAS detector (2016). ATLAS-CONF-2016-010.
- [37] Search for high-mass resonances in $Z\gamma \rightarrow e^+e^-\gamma/\mu^+\mu^-\gamma$ final states in proton-proton collisions at $\sqrt{s} = 13 \text{ TeV}$ (2016). CMS-PAS-EXO-16-019.
- [38] G. Aad, et al., Search for high-mass diphoton resonances in pp collisions at $\sqrt{s} = 8 \text{ TeV}$ with the ATLAS detector, Phys. Rev. D92 (2015) 032004.
- [39] G. Aad, et al., Search for an additional, heavy Higgs boson in the $H \rightarrow ZZ$ decay channel at $\sqrt{s} = 8 \text{ TeV}$ in pp collision data with the ATLAS detector, Eur. Phys. J. C76 (2016) 45.
- [40] G. Aad, et al., Search for new resonances in $W\gamma$ and $Z\gamma$ final states in pp collisions at $\sqrt{s} = 8 \text{ TeV}$ with the ATLAS detector, Phys. Lett. B738 (2014) 428–447.
- [41] G. Aad, et al., Search for new phenomena in the dijet mass distribution using $p-p$ collision data at $\sqrt{s} = 8 \text{ TeV}$ with the ATLAS detector, Phys. Rev. D91 (2015) 052007.
- [42] G. Aad, et al., Search for new phenomena in dijet mass and angular distributions from pp collisions at $\sqrt{s} = 13 \text{ TeV}$ with the ATLAS detector, Phys. Lett. B754 (2016) 302–322.
- [43] V. Khachatryan, et al., Search for narrow resonances decaying to dijets in proton-proton collisions at $\sqrt{s} = 13 \text{ TeV}$, Phys. Rev. Lett. 116 (2016) 071801.
- [44] Search for an Higgs Like resonance in the diphoton mass spectra above 150 GeV with 8 TeV data (2014). CMS-PAS-HIG-14-006.

- [45] V. Khachatryan, et al., Search for a Higgs Boson in the Mass Range from 145 to 1000 GeV Decaying to a Pair of W or Z Bosons, *JHEP* 10 (2015) 144.
- [46] Search for scalar resonances in the 200–1200 GeV mass range decaying into a Z and a photon in pp collisions at $\sqrt{s} = 8$ TeV (2016). CMS-PAS-HIG-16-014.
- [47] Search for Resonances Decaying to Dijet Final States at $\sqrt{s} = 8$ TeV with Scouting Data (2015). CMS-PAS-EXO-14-005.
- [48] G. Aad, et al., Search for pair-produced third-generation squarks decaying via charm quarks or in compressed supersymmetric scenarios in pp collisions at $\sqrt{s} = 8$ TeV with the ATLAS detector, *Phys. Rev. D* 90 (2014) 052008.
- [49] V. Khachatryan, et al., Search for dark matter, extra dimensions, and unparticles in monojet events in proton-proton collisions at $\sqrt{s} = 8$ TeV, *Eur. Phys. J. C* 75 (2015) 235.
- [50] J. Alwall, M. Herquet, F. Maltoni, O. Mattelaer, T. Stelzer, *MadGraph 5 : Going Beyond*, *JHEP* 06 (2011) 128.
- [51] J. Alwall, R. Frederix, S. Frixione, V. Hirschi, F. Maltoni, O. Mattelaer, H. S. Shao, T. Stelzer, P. Torrielli, M. Zaro, The automated computation of tree-level and next-to-leading order differential cross sections, and their matching to parton shower simulations, *JHEP* 07 (2014) 079.
- [52] L. A. Harland-Lang, V. A. Khoze, M. G. Ryskin, The production of a diphoton resonance via photon-photon fusion, *JHEP* 03 (2016) 182.
- [53] A. Alloul, N. D. Christensen, C. Degrande, C. Duhr, B. Fuks, *FeynRules 2.0 - A complete toolbox for tree-level phenomenology*, *Comput. Phys. Commun.* 185 (2014) 2250–2300.
- [54] SM Higgs Branching Ratios and Partial-Decay Widths., 2016.
- [55] M. Sher, Electroweak Higgs Potentials and Vacuum Stability, *Phys. Rept.* 179 (1989) 273–418.
- [56] J. Elias-Miro, J. R. Espinosa, G. F. Giudice, H. M. Lee, A. Strumia, Stabilization of the Electroweak Vacuum by a Scalar Threshold Effect, *JHEP* 06 (2012) 031.
- [57] S. Alekhin, A. Djouadi, S. Moch, The top quark and Higgs boson masses and the stability of the electroweak vacuum, *Phys. Lett. B* 716 (2012) 214–219.
- [58] D. Buttazzo, G. Degrande, P. P. Giardino, G. F. Giudice, F. Sala, A. Salvio, A. Strumia, Investigating the near-criticality of the Higgs boson, *JHEP* 12 (2013) 089.
- [59] G. Aad, et al., Search for heavy neutrinos and right-handed W bosons in events with two leptons and jets in pp collisions at $\sqrt{s} = 7$ TeV with the ATLAS detector, *Eur. Phys. J. C* 72 (2012) 2056.
- [60] V. Khachatryan, et al., Search for heavy neutrinos and W bosons with right-handed couplings in proton-proton collisions at $\sqrt{s} = 8$ TeV, *Eur. Phys. J. C* 74 (2014) 3149.
- [61] J. Jaeckel, M. Jankowiak, M. Spannowsky, LHC probes the hidden sector, *Phys. Dark Univ.* 2 (2013) 111–117.
- [62] S. Chatrchyan, et al., A search for a doubly-charged Higgs boson in pp collisions at $\sqrt{s} = 7$ TeV, *Eur. Phys. J. C* 72 (2012) 2189.
- [63] G. Aad, et al., Search for doubly-charged Higgs bosons in like-sign dilepton final states at $\sqrt{s} = 7$ TeV with the ATLAS detector, *Eur. Phys. J. C* 72 (2012) 2244.
- [64] G. Aad, et al., Search for anomalous production of prompt same-sign lepton pairs and pair-produced doubly charged Higgs bosons with $\sqrt{s} = 8$ TeV pp collisions using the ATLAS detector, *JHEP* 03 (2015) 041.
- [65] J. P. Araque Espinosa, N. Castro, J. Santiago, A. M. Onofre, Search for heavy fermions with the ATLAS experiment at the LHC collider, (2015). CERN-THESIS-2015-330.
- [66] M. Spira, A. Djouadi, D. Graudenz, P. M. Zerwas, Higgs boson production at the LHC, *Nucl. Phys. B* 453 (1995) 17–82.